Volume 1 | Number 1 | Jan 2013 | Pages 1–100

Nanoscale

www.rsc.org/nanoscale

ROYAL SOCIETY OF CHEMISTRY

This is an *Accepted Manuscript*, which has been through the Royal Society of Chemistry peer review process and has been accepted for publication.

Accepted Manuscripts are published online shortly after acceptance, before technical editing, formatting and proof reading. Using this free service, authors can make their results available to the community, in citable form, before we publish the edited article. We will replace this *Accepted Manuscript* with the edited and formatted *Advance Article* as soon as it is available.

You can find more information about *Accepted Manuscripts* in the **Information for Authors**.

Please note that technical editing may introduce minor changes to the text and/or graphics, which may alter content. The journal's standard **Terms & Conditions** and the **Ethical guidelines** still apply. In no event shall the Royal Society of Chemistry be held responsible for any errors or omissions in this *Accepted Manuscript* or any consequences arising from the use of any information it contains.

Journal Name

ARTICLE

Light-Controlled Propulsion, Aggregation and Separation of Water-Fuelled TiO₂/Pt Janus Submicromotors and Their "on-the-fly" Photocatalytic Activities

Fangzhi Mou,† Lei Kong,† Chuanrui Chen, Zhihong Chen, Leilei Xu and Jianguo Guan*

In this work, the water-fuelled TiO₂/Pt Janus submicromotors with light-controlled motions have been developed by utilizing the asymmetrical photocatalytic water redox reaction over TiO₂/Pt Janus submicrospheres under UV irradiation. The motion state, speed, aggregation and separation behaviors of the TiO₂/Pt Janus submicromotor can be reversibly, wirelessly and remotely controlled at will by regulating "on/off" switch, intensity and pulsed/continuous irradiation mode of UV light. The motion of the water-fuelled TiO₂/Pt Janus submicromotor is governed by the light-induced self-electrophoresis under the local electrical field generated by the asymmetrical water oxidation and reduction reactions on its surface. The TiO₂/Pt Janus submicromotors can interact with each other through the light-swithable electrostatic forces, and hence using the continuous and pulsed UV irradiation can have the TiO₂/Pt Janus submicromotors to aggregate and separate at will, respectively. Because of the enhanced mass exchange between the environment and active submicromotors, the separated TiO₂/Pt Janus submicromotors powered by the pulsed UV irradiation show a much higher activity for the photocatalytic degradation of the organic dye than the aggregated TiO₂/Pt submicromotors. The water-fuelled TiO₂/Pt Janus submicromotors developed here have some outstanding advantages as "swimming" photocatalysts for organic pollutant remediation in macro or microenvironment (microchannels and microwells in microchips) because of their small size, long-term stability, wirelessly controllable motion behaviors and long life span.

Introduction

Chemically powered micro/nanomotors may have fascinating capabilities to pick up, transport, and release various micro/nanocargoes in liquid media. Thus, they can perform complex tasks, including drug delivery, protein and cell separation, microsurgeries and environmental remediation, etc. if they are steered in a controllable way, involving activation, acceleration, deceleration or stop etc..[1-9] Up to now, various micro/nanomotors, such as the asymmetrical catalytic nanorods,[10, 11] spherical Janus micromotors,[12-15] pot-like micromotors[16] and tubular microengines,[17, 18] have been developed based on bubble propulsion and self-phoresis, and it has already been demonstrated that their motions can be controlled by magnetic field, electrical field, ultrasound field, light, heat pulse and fuel gradient.[19-29] However, extra fuel sources, such as H₂O₂, acidic, alkaline, Br₂, or I₂ solutions, are usually needed to be introduced into the ambience to power the micro/nanomotors, and they are considered to be incompatible with living organisms and harmful for the environment. Therefore, micro/nanomotors that can harvest energy from their own surrounding environment, i.e., use water as their fuel source, are highly desired.[30-33]

Cooperative arrangements of individual micro/nanomotors, such as aggregation and assembly, may create machine groups that can cooperatively perform complex tasks that a single micro/nanomotor is impossible to carry out.[34-36] However, since the size increment of motor aggregates will make the drag force increase, the aggregation of separated micro/nanomotors may seriously reduce their speed, affecting their efficiency for the cargo transportation or "on-the-fly" adsorption and degradation.

In this work, taking into account the excellent photocatalytic activity and high stability of TiO₂/Pt heterostructures,[37-39] we have demonstrated a TiO₂/Pt Janus submicromotor by utilizing the photocatalytic water redox reaction over TiO₂/Pt under UV irradiation. The motion state, speed, aggregation and separation behaviors of the TiO₂/Pt Janus submicromotor can be reversibly, wirelessly and remotely controlled at will by regulating the "on/off" switch, intensity and pulsed/continuous irradiation mode of UV light. The propulsion mechanism is attributed to the light-controlled self-electrophoretic motion of the negatively charged TiO₂/Pt Janus submicromotor. Due to the separation of the photogenerated charge pairs in TiO₂/Pt heterojunctions, the TiO₂ and Pt components of the TiO₂/Pt Janus submicromotor are

ª· State Key Laboratory of Advanced Technology for Materials Synthesis and Processing, Wuhan University of Technology; 122 Luoshi Road, Wuhan 430070, China; Fax: (+86)-27-87879468, E-mail: guanjg@whut.edu.cn.
† These authors contribute equally in this work.

ARTICLE   **Journal Name**

oppositely charged under UV irradiation, forming compact aggregates of the TiO₂/Pt Janus submicromotors through the electrostatic attraction between the TiO₂ and Pt components of the neighboring motors. The aggregated submicromotors could be relaxed into separated ones again by Brownian motion when the UV irradiation is off. In this way, using continuous and pulsed UV irradiation can control the aggregation and separation of the TiO₂/Pt Janus submicromotors at will, respectively. Because of the enhanced mass exchange between the environment and active submicromotors, the separated TiO₂/Pt Janus submicromotors powered by the pulsed UV irradiation show a much higher activity for the photocatalytic degradation of the organic dye than that of the aggregated TiO₂/Pt submicromotors. Compared to the self-propelled water-fuelled Mg/Au-TiO₂ Janus micromotors based on the corrosion reaction of metal Mg,[33] the water-fuelled TiO₂/Pt Janus submicromotors have an outstanding advantage of the long life-time in the on-the-fly degradation of organic pollutants.

Experimental Section

Preparation of TiO₂ submicrospheres. Monodisperse TiO₂ submicrospheres with size of 800 nm were prepared according to the previous report.[40] Briefly, 50 mL of ethanol was mixed with 0.2 mL of sodium chloride solution (0.4 mM), followed by addition of 0.85 mL of tetrabutyl titanate at ambient temperature. After 5 min of stirring, the solution was allowed to stand for another 2 hours. The resulted TiO₂ submicrospheres were then collected after centrifugation and washed with ethanol for three times. TiO₂ microspheres with size of 3.5 and 7 μm were prepared according to the previous report.[41]

Preparation of TiO₂/Pt submicrospheres. A 0.5 mL TiO₂ ethanol/butanol (0.95/0.05 in volume) suspension was dropped onto a modified glass slide, which was previously cleaned with Piranha solution and washed by deionized water, and dried at ambient temperature. Then, the TiO₂ submicrospheres on the glass slide were sintered at 450 °C for 2 hours to obtain anatase TiO₂ submicrospheres. The anatase TiO₂ submicrospheres were partially covered with a platinum layer (about 30 nm in thickness) by ion sputtering for 300 s under a pressure of 0.6 Pa (Model E-1020 Hitachi ion sputter). Finally, the TiO₂/Pt Janus submicrospheres were obtained by sonicating the glass slide in deionized water for 5 s. SiO₂/Pt microspheres were prepared by simply replacing TiO₂ submicroparticles by SiO₂ spheres (Aladdin Co., China) with size of 1 μm in the platinum sputtering process.

Characterization of TiO₂/Pt submicrospheres. Scanning electron microscopy (SEM) and energy-dispersive X-ray (EDX) spectroscopy were obtained using a Hitachi S-4800 Field-emission SEM (Japan). The X-ray diffraction (XRD) patterns of the samples were recorded on a Rigaku D/Max-2000 diffractometer.

Recording microscopy videos and analysis. 100 μL aqueous suspension containing TiO₂/Pt Janus submicrospheres was spread on a glass slide. A UV-LED light source with a

wavelength of 368 nm was placed 2.0 cm above the surface of suspension, and the UV intensity on the surface of the suspension is 1 W cm⁻². The motions of the TiO₂/Pt Janus submicrospheres under the continuous or pulsed UV irradiation with different intensities were observed and recorded at room temperature through an optical microscope (Leica DMI 3000M). All videos of the motion of the submicromotors were analyzed by using Video Spot Tracker V08.01 software.

Photocatalytic activities. A 96-well plate was used to study the photocatalytic degradation of Rhodamine B (RhB) under different motion state of the TiO₂/Pt Janus submicromotors. For the photocatalytic degradation of RhB by the moving TiO₂/Pt submicromotors under continuous and pulsed UV irradiation, 100 μL aqueous suspension containing 2×10^6 pcs/ml TiO₂/Pt submicrospheres and 20 μM RhB was added into two wells of the 96-well plate, and then irradiated by continuous and pulsed (3 s-0.5 s UV on-off cycle) UV light (1 W cm⁻²) for 80 min, respectively. Fluorescent images of the RhB solution were taken every 10 min by the fluorescent microscope (Leica DMI 3000M). The degradation of the RhB was evaluated by analyzing the decreasing fluorescent intensity of the solution through the image analysis program (Adobe Photoshop). The relationship between fluorescent intensity and concentration of RhB was also studied.
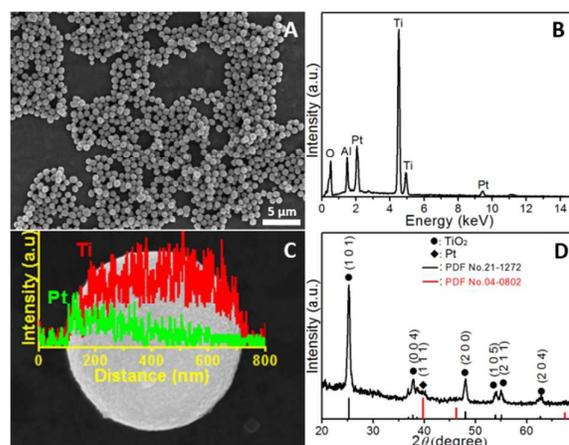
Results and Discussion

Figure 1. (A) SEM image, (B) EDX Spectrum of the TiO₂/Pt Janus submicromotors; (C) linear EDX analysis of Pt and Ti over a typical TiO2/Pt submicromotor; (D) XRD pattern of the TiO₂/Pt Janus submicromotors.

The TiO₂/Pt Janus submicromotors are fabricated by asymmetrically coating a platinum layer on the exposed surfaces of the anatase TiO₂ submicrospheres on a flat glass substrate via ion sputtering process. Figure 1A shows the TiO₂/Pt Janus submicromotors on the substrate, suggesting they have an average size of 800 nm. The TiO₂/Pt Janus submicromotors were then peel off from the substrate by ultrasonication in water for 5 s. The EDX analysis (Figure 1B) confirms that the TiO₂/Pt Janus submicromotors mainly consist of titanium, oxygen and platinum. The elemental linear EDX

analysis (Figure 1C) for a typical TiO_2/Pt submicromotor indicates that Pt is asymmetrically distributed on the TiO_2 submicrosphere, confirming the Janus structure of the TiO_2/Pt submicromotors. The XRD pattern in Figure 1D indicates that TiO_2 in the TiO_2/Pt submicromotors have a well-crystalline anatase phase (PDF No. 21-1272). The weak peak at 39.8^o can be assigned to metal Pt (PDF No. 04-0802). Zeta potential measurement reveals that the anatase TiO_2 submicrospheres and TiO_2/Pt Janus submicromotors have a negative surface charge of -7 and -12 mV, respectively.

Figure 2A shows that the TiO_2/Pt Janus submicromotors exhibit random Brownian motions when the UV irradiation is off. When the UV irradiation (1 W cm^{-2}) is turned on, the ballistic motion of the submicromotors is activated, as shown in Figure 2B and SI-Video 1. The average speed of the submicromotors is 21 μm s^{-1}, about 26 body length per second, suggesting the strong driving force of the submicromotor. The "on/off" propulsion of the submicromotors is reversible by turning on or off the UV irradiation. The submicromotor is observed to have a long lifetime due to the high stability of both TiO_2/Pt submicrospheres and their photocatalytic water splitting reactions.
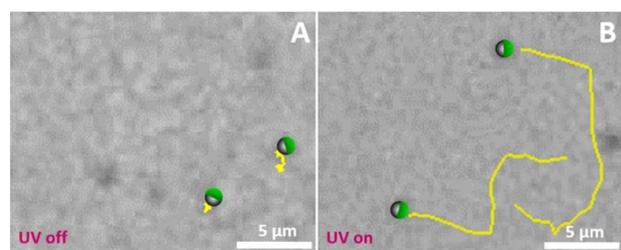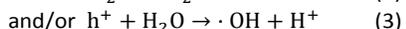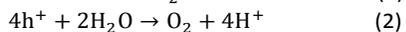

Figure 2. Trajectories of two typical TiO_2/Pt submicromotors in water (A) without and (B) with UV irradiation within a period of 1 s. For easy identification, the black dots in the microscopic images, corresponding to submicromotors, are replaced by two schematic diagrams of Janus submicrospheres, and the trajectories of the submicromotors are depicted as yellow curves.

The TiO_2/Pt heterostructure has an excellent photocatalytic activity and high stability for photocatalytic water splitting under UV irradiation because noble metal Pt can act as an electron acceptor to suppress the recombination of electron-hole pairs and enhance their lifetime.[42] As shown in Figure 3A, under UV irradiation, the photogenerated electrons in the TiO_2 are transferred to the Pt layer for water reduction, and the photogenerated holes engage in the water oxidation on the exposed TiO_2 surface according to Equation 1-3.[43]

$$2e^- + 2H^+ \rightarrow H_2 \qquad (1)$$
$$4h^+ + 2H_2O \rightarrow O_2 + 4H^+ \qquad (2)$$
$$\text{and/or } h^+ + H_2O \rightarrow \cdot OH + H^+ \qquad (3)$$

Thus, H^+ is highly concentrated on the TiO_2 side, and a local electric field pointing from the TiO_2 end to the Pt end is formed.[44] On the other hand, the photogenerated holes in the valence band (VB) of TiO_2 are thermodynamically below the O_2/H_2O redox potential by 2 eV, while electrons in the conduction band (CB) are above the H^+/H_2 potential only by 0.1-0.2 eV. Hence, in the photocatalytic water redox reaction by the TiO_2/Pt heterostructures, the photogenerated holes in

the VB of TiO_2 can quickly oxidize water via Equation 2 and/or 3 within 2 μs, whereas the electrons tend to accumulated in the Pt component since the water reduction with the electrons via Equation 1 is slow and usually takes about 10-900 μs.[45] Consequently, the charge separation has the TiO_2 and Pt component charged positively and negatively under UV irradiation, respectively (Figure 3A), but the whole TiO_2/Pt Janus submicromotor exhibits a net negative charge. This is confirmed by Figure S1, which indicates the same electrophoretic motion direction of the TiO_2/Pt Janus submicromotors under an electric field with or without UV irradiation, respectively. The negatively charged TiO_2/Pt Janus submicromotor could be driven by the local electric field with the TiO_2 side forward via the electrophoresis (Figure 3A) according to Equation 4.[46]

$$V = \zeta \varepsilon E / \mu \qquad (4)$$

Here, ζ represents the zeta potential of the Janus submicrosphere. E is the generated electric field. ε and μ are the permittivity and viscosity of the aqueous medium, respectively.
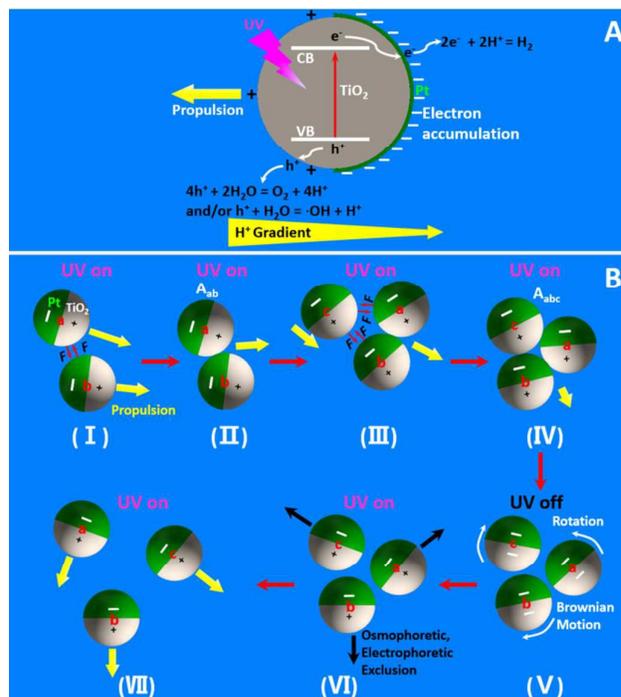

Figure 3. Schematic diagrams of (A) the propulsion mechanism of the water-fuelled TiO_2/Pt submicromotor (in a cross section type), and (B) the aggregation and separation of the TiO_2/Pt Janus submicromotors through light-switchable electrostatic interactions: (I-IV) TiO_2/Pt Janus submicromotors approach each other and aggregate under UV irradiation due to the electrostatic attraction between the TiO_2 and Pt components in neighboring motors; (V) the aggregated TiO_2/Pt Janus submicromotors are relaxed under Brownian motions when the UV irradiation is off; (VI and VII) the relaxed submicromotors are then separated due to the osmophoretic and electrophoretic exclusion and the light-induced motion when the UV is back on.

As single-component TiO_2 submicrospheres cannot effectively separate the photogenerated charge pairs and make the subsequent asymmetrical water redox reactions, no obvious speed variation is observed for them in water with or without

UV irradiation (SI-Video 2). This further confirms that the Janus structure and the asymmetrical water redox reactions on the surface play a key role for the self-electrophretic propulsion of the TiO$_2$/Pt Janus submicromotors. Sen and co-workers have demonstrated a light-triggered motion of the irregular commercial TiO$_2$ particles in water under UV irradiation.[21] Even though they did not discuss the detailed propulsion mechanism in their work, it is believed that the asymmetrical water redox reactions occurred since the irregular commercial TiO$_2$ particles consist of anatase/rutile heterostructures, in which the photogenerated electrons and holes are separated and enriched respectively in rutile and anatase phases for water reduction and oxidation,[47] thus creating a local electric field to propel the negatively charged TiO$_2$ particles.
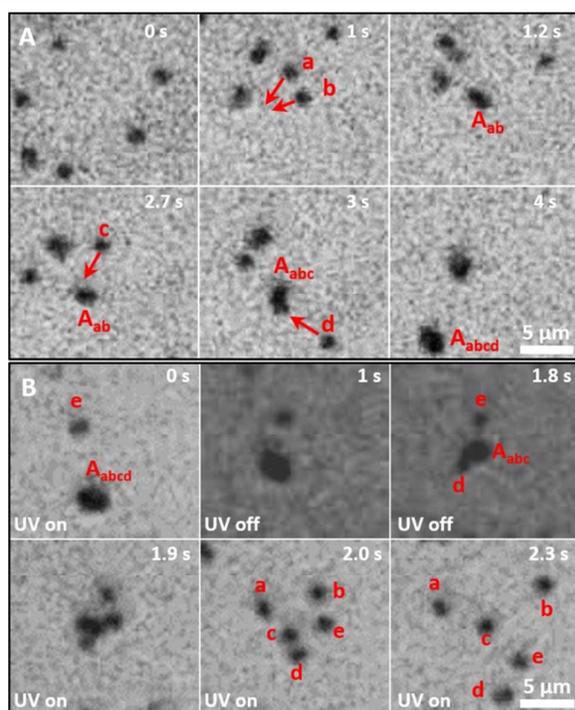

Figure 4. (A) The aggregation behaviors of the TiO$_2$/Pt Janus submicromotors (a, b, c and d) in water under continuous UV irradiation, leading to the formation of the aggregates (A$_{ab}$, A$_{abc}$ and A$_{abcd}$) at different time intervals; (B) the separation of the aggregate (A$_{abcd}$) into separated submicromotor s (a, b, c and d) in an UV on-off-on cycle at different time intervals.

The light could also induce the photothermal effect of the submicromotors, which may create a local temperature gradient across the submicromotors, and propel it move forward through thermophoresis.[48] To evaluate the contribution of the photothermal effect on the light-controlled motion of the TiO$_2$/Pt submicromotors, we have tested the photothermal effect of the TiO$_2$ and TiO$_2$/Pt submicroparticles. The results in Figure S2 indicate that the metal Pt layer has a much stronger photothermal conversion than the TiO$_2$ submicroparticles. However, the photothermal conversion of the metal Pt layer is too low to power the submicromotor through thermophoresis, as evidenced by the fact that the SiO$_2$/Pt microparticles show no directional motion in water

under UV irradiation (SI-Video 3). Hence, the light-controlled propulsion of the motors originate from the photocatalytic chemical reactions rather than the photothermal effect. On the other hand, the photothermal effect of the submicromotors can cause the temperature rise of the submicromotors and environment and thus increase the reaction rate of the photocatalysis,[26] to some extent contributing to the motion of the TiO$_2$/Pt submicromotors.

According to Equation 4, the speed of the micromotros is propotional to E, which is determined by the [H$^+$] gradient created by the photocatalytic water redox reaction. As adjusting the intensity (I) of the UV irradiation can change the photon flux (Φ, the number of incident photons per second per unit area) on the submicromotor, and thus the number of the photogenerated holes and electrons for the water redox reactions, the rate of the water redox reactions and the speed of the submicromotors could be modulated in this way. Figure S3 shows that when I increases from 0.1 to 1 W cm^{-2}, the average speed of the submicromotor increases from 4 to 21 μm s^{-1}, confirming the dependence of the speed of the submicromotor on the UV intensity. The speed of the TiO$_2$/Pt submicromotors is also sensitive to their sizes. As shown in Figure 2 and S4, when the motor size is increased from 0.8, 3.5 to 7 μm, the motion speed decreases obviously from 21, 9 to 2.5 μm s^{-1} (SI-Video 4). This can be attributed to the increasing viscous drag force (F_d) with the size according to Equation 5.

$$F_d = 6\pi r\eta v \qquad (5)$$

Here, r and v are the radius and speed of the TiO$_2$/Pt micromotors. η is the dynamic viscosity of the water.
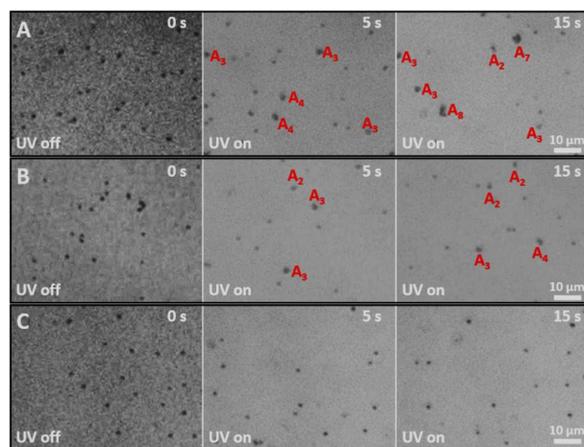

Figure 5. The formation of submicromotor aggregates (A$_x$, x=1-8, representing the numbers of aggregated submicromotors) under (A) continuous UV irradiation, and (B, C) pulsed UV irradiation with (B) 1 s-0.1 s and (C) 1 s-0.5 s on-off cycles at different time intervals.

Under UV irradiation the photogenerated electrons within the TiO$_2$/Pt Janus heterostructures will be transferred to the Pt layer, making it charged oppositely to the TiO$_2$ component. As a result, the TiO$_2$/Pt Janus submicromotors tend to form a compact aggregate due to the electrostatic attraction between the TiO$_2$ and Pt components of the neighboring submicromotors when they approach. As shown in Figure 4A and SI-Video 5 (in 2X slow motion), two moving

submicromotors (a and b) approach with each other and form into a moving dimer (A_{ab}). When more submicromotors collide with A_{ab} step by step, the trimer (A_{abc}) or tetramer (A_{abcd}) can also be formed. Figure 3B shows the schematic diagram of the aggregation process of the moving submicromotors in steps of I-IV. In some rare cases, when two TiO_2/Pt Janus submicromotors approaches with each other face-to-face, they repel each other instead of forming an aggregate due to the electrostatic repulsion between the two positive charged TiO_2 surfaces (SI-Video 6 and Figure S5), further confirming that the aggregation of the TiO_2/Pt Janus submicromotors is attributed to the electrostatic attraction between the different components of the approaching submicromotors.

When the UV irradiation is off, no fresh electron-hole pairs are photogenerated in the submicromotors. In this case, both TiO_2 and Pt components are negatively charged, leading the aggregated submicromotors to electrostatically repel each other and easily make them separately rotate under Brownian motion (0-1.8 s in Figure 4B and V in Figure 3B). According to the Einstein-Smoluchowski equation, the mean square displacement produced by the Brownian motion follows $X^2 = 4Dt$ under equilibrium, where D is the diffusion coefficient, and t represents the time.[49] Hence, the distance (d) between the neighboring submicromotors is enlarged with prolonging the UV off time. It is interesting to note that when UV irradiation is back on, the loosely aggregated submicromotors do not instantly form into compact aggregates. Instead, they move away from each other and have the distance (d) between the neighboring submicromotors further expanded, as shown in 1.9-2.3 s in Figure 4B. This could be explained by the following 3 reasons. Firstly, the electrostatic forces (F) between two neighboring TiO_2/Pt Janus submicromotors can be described using Equation 6:

$$F = \frac{Q_1 Q_2}{4\pi\varepsilon R(r+d+R)^2}\left[R + \frac{\sqrt{(d+r)^2+2(r+d+R)R}}{2} - \frac{(d+r)(d+r+2R)}{2\sqrt{(r+d)^2+2(r+d+R)R}}\right] \quad (6)$$

Where Q_1 and Q_2 are the charges on two separated hemispherical surfaces of neighboring submicromotors (Figure S6), r and R are the radius of the submicromotors. More detailed calculation process is provided in Supporting Information. According to Equation 5, it is obvious that the electrostatic attractive forces (F) between the loosely aggregated submicromotors decreases remarkably compared to that between the tightly aggregated ones, preventing the direct aggregation of the submicromotors through electrostatic attraction. More importantly, there occur the osmophoretic and electrophoretic exclusive motions at the early stage of their re-activation by UV irradiation. Namely, the photocatalytically generated H_2 would be highly concentrated in the confined interparticle spaces when UV irradiation is back on, creating local osmophoretic flows to push the submicromotors away from each other according to $U=b\nabla C$, where U is the speed of submicromotors, b is the slip-veocity coeffient, and ∇C is the concentration gradient of the

photocatalytically generated H_2.[46] Furthermore, since H^+ has a higher diffusion rate than those anions, such as OH^- and $\cdot O_2^-$ (the resultants of the reaction between the photogenerated e^- and dissolved oxygen), a temporary electric field is built up around the aggregate, which can also drive the negatively-charged submicromotors away from each other. This is similar to the exclusion process of negatively-charged SiO_2 tracer particles by the TiO_2-based micropump reported by Sen and co-workers.[21] Consequently, the re-activated submicromotors in the aggregate move away along different directions separately, as shown in VI-VII of Figure 3B and SI-Video 5. Finally, the random Brownian motions of the submicromotors may also play a positive role in preventing them from immediately re-colliding with each other due to the change of the motion direction when they are re-activated.
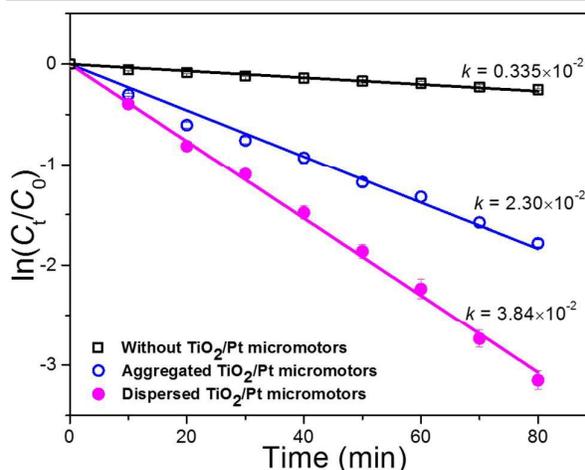

Figure 6. The photocatalytic degradation of RhB by the aggregated and separated TiO_2/Pt Janus submicromotors under continuous and pulsed (3 s-0.5 s on-off) UV irradiation, respectively.

From the aggregation-separation behaviors of the TiO_2/Pt Janus submicromotors in one UV irradiation on-off-on cycle (Figure 4B) and the underlying mechanism, the aggregation of the submicromotors may be avoided by using pulsed UV irradiation. Figure 5A and SI-Video 7 show that when continuous UV irradiation is used to power the TiO_2/Pt Janus submicromotors, a large number of aggregates consisting of 3-8 submicromotors could be formed in 15 s. When a pulsed UV irradiation with 1 s on-0.1 s off repeating cycles is used, the number and size of aggregates are reduced, but there still exist motor aggregates (Figure 5B and SI-Video 7). However, when a pulsed UV irradiation with 1 s on-0.5 s off repeating cycles is used, no aggregate is formed, as shown in Figure 5C and SI-Video 7. These results reveal that we can control the aggregation and separation of the moving TiO_2/Pt Janus submicromotors using continuous and pulsed UV irradiation, respectively. The continuous existence of motor aggregates under the pulsed UV irradiation with 1 s on-0.1 s off repeating cycles could be attributed to the assumption that some aggregates there have a relaxation time longer than 0.1 s. This can be affirmed by the disappearance of aggregates under the pulsed UV irradiation with 1 s on-0.5 s off repeating cycles,

which gives the aggregated submicromotors 0.5 s to relax under Brownian motion.

Because of the light-controlled motion of the water-fuelled TiO_2/Pt Janus submicromotors, they could act as efficient "swimming" photocatalysts for the degradation of organic pollutants in water. The photocatalytic activity of the water-fuelled TiO_2/Pt Janus submicromotors was evaluated by photocatalytic degradation of RhB aqueous solution under UV irradiation. The light-induced motions of the submicromotors in 20 µM RhB solution under continuous and pulsed UV irradiation are given in SI-Video 8, which also indicates that the pulsed UV irradiation can effectively inhibit the aggregation of the submicromotors. As shown in Figure 6, the degradation of RhB follows the first-order kinetics mode (Equation 7).

$$\ln\left(\frac{C_t}{C_0}\right) = kt \qquad (7)$$

where C_0 and C_t are the original concentration and that at the UV irradiation time of t. k is the first-order rate constant.

It can be seen that the photodegradation rate of RhB under UV irradiation without micrmotors is rather slow with a k of 0.34×10^{-2} min^{-1}. For the RhB solution containing the TiO_2/Pt Janus submicromotors under continuous UV irradiation, the photodegradation rate of RhB reaches 2.30×10^{-2} min^{-1}, indicating the presence of submicromotors is crucial for the degradation process. Interestingly, the photodegradation rate of RhB by the moving TiO_2/Pt Janus submicromotors under pulsed irradiation is much higher than that under continuous UV irradiation (3.84×10^{-2} vs. 2.30×10^{-2} min^{-1}). This can be explained by the fact that the moving TiO_2/Pt Janus submicromotors tend to form aggregates under continuous UV irradiation, reducing their speed, which retards the mass exchange between the motor and the environment, and hence lower their activity in the "on-the-fly" photocatalytic degradation for RhB. In comparison, no aggregates can be formed if the pulsed UV irradiation is used to power the TiO_2/Pt Janus submicromotors. Hence, the separated submicromotors powered by the pulsed UV irradiation can actively attack RhB molecules because they have a higher average speed than those aggregated submicromotors, which facilitates the efficient dispersion of the photogenerated reactive oxidative species (·OH etc.) and their interaction with the target RhB molecules.[7, 33] Compared to the self-propelled water-driven Mg/Au-TiO_2 Janus micromotors based on the corrosion reaction of metal Mg,[33] the water-fuelled TiO_2/Pt Janus submicromotors have an outstanding advantage of the long life-time in the on-the-fly degradation of organic pollutants because of the high stability of the TiO_2/Pt Janus submicromotors and their photocatalytic reactions.

Conclusions

In conclusion, we have demonstrated water-fuelled TiO_2/Pt Janus submicromotors by utilizing the photocatalytic water redox reaction over TiO_2/Pt under UV irradiation. The motion state, speed, aggregation and separation behaviors of the TiO_2/Pt Janus submicromotor can be reversibly, wirelessly and remotely controlled at will by regulating "on/off" switch, intensity and pulsed/continuous irradiation mode of UV. The motion of the water-fuelled TiO_2/Pt Janus submicromotors is governed by the light-induced self-electrophoresis under the local electrical field generated by the asymmetrical surface water oxidation and reduction reactions. The TiO_2/Pt Janus submicromotors can interact with each other through the light-swithable electrostatic forces, and hence the aggregation and the separation of the TiO_2/Pt Janus submicromotors can be controlled at will by using continuous and pulsed UV irradiation, respectively. Because of the enhanced mass exchange between the environment and active submicromotors, the separated TiO_2/Pt Janus submicromotors powered by the pulsed UV irradiation show a much higher activity for the photocatalytic degradation of the organic dye than that of the aggregated TiO_2/Pt submicromotors. The water-fuelled TiO_2/Pt Janus submicromotors developed in this work have some outstanding advantages as "swimming" photocatalysts for organic pollutant remediation in macro or microenvironment (microchannels and microwells in microchips) because of their small size, high stability, wirelessly controllable motion behaviors and long life span.

Notes and references

1. J. Wang, *Nanomachines: Fundamentals and Applications*, Wiley, 2013.
2. S. Sanchez, L. Soler and J. Katuri, *Angew. Chem. Int. Ed.*, 2015, **54**, 1414-1444.
3. M. Guix, C. C. Mayorga-Martinez and A. Merkoçi, *Chem. Rev.*, 2014, **114**, 6285-6322.
4. D. Patra, S. Sengupta, W. Duan, H. Zhang, R. Pavlick and A. Sen, *Nanoscale*, 2013, **5**, 1273-1283.
5. S. Sengupta, M. E. Ibele and A. Sen, *Angew. Chem. Int. Ed.*, 2012, **51**, 8434-8445.
6. W. Wang, W. Duan, S. Ahmed, T. E. Mallouk and A. Sen, *Nano Today*, 2013, **8**, 531-554.
7. W. Gao and J. Wang, *ACS Nano*, 2014, **8**, 3170-3180.
8. V. Magdanz, M. Guix and O. Schmidt, *Robotics and Biomimetics*, 2014, **1**, 1-10.
9. J. Wang and K. M. Manesh, *Small*, 2010, **6**, 338-345.
10. W. F. Paxton, K. C. Kistler, C. C. Olmeda, A. Sen, S. K. St. Angelo, Y. Cao, T. E. Mallouk, P. E. Lammert and V. H. Crespi, *J. Am. Chem. Soc.*, 2004, **126**, 13424-13431.
11. R. Liu and A. Sen, *J. Am. Chem. Soc.*, 2011, **133**, 20064-20067.
12. J. R. Howse, R. A. L. Jones, A. J. Ryan, T. Gough, R. Vafabakhsh and R. Golestanian, *Phys. Rev. Lett.*, 2007, **99**, 048102.

ARTICLE

13. L. Baraban, M. Tasinkevych, M. N. Popescu, S. Sanchez, S. Dietrich and O. G. Schmidt, *Soft Matter*, 2012, **8**, 48-52.

14. L. Baraban, D. Makarov, R. Streubel, I. Moench, D. Grimm, S. Sanchez and O. G. Schmidt, *ACS Nano*, 2012, **6**, 3383-3389.

15. W. Gao, M. D'Agostino, V. Garcia-Gradilla, J. Orozco and J. Wang, *Small*, 2013, **9**, 467-471.

16. F. Mou, D. Pan, C. Chen, Y. Gao, L. Xu and J. Guan, *Adv. Funct. Mater.*, 2015, DOI: 10.1002/adfm.201502835.

17. A. A. Solovev, Y. F. Mei, E. B. Urena, G. S. Huang and O. G. Schmidt, *Small*, 2009, **5**, 1688-1692.

18. Y. F. Mei, A. A. Solovev, S. Sanchez and O. G. Schmidt, *Chem. Soc. Rev.*, 2011, **40**, 2109-2119.

19. F. Mou, Y. Li, C. Chen, W. Li, Y. Yin, H. Ma and J. Guan, *Small*, 2015, **11**, 2564-2570.

20. P. Calvo-Marzal, K. M. Manesh, D. Kagan, S. Balasubramanian, M. Cardona, G.-U. Flechsig, J. Posner and J. Wang, *Chem. Commun.*, 2009, 4509-4511.

21. Y. Y. Hong, M. Diaz, U. M. Cordova-Figueroa and A. Sen, *Adv. Funct. Mater.*, 2010, **20**, 1568-1576.

22. S. Giudicatti, S. M. Marz, L. Soler, A. Madani, M. R. Jorgensen, S. Sanchez and O. G. Schmidt, *J. Mater. Chem. C*, 2014, **2**, 5892-5901.

23. J. Palacci, S. Sacanna, A. P. Steinberg, D. J. Pine and P. M. Chaikin, *Science*, 2013, **339**, 936-940.

24. J. Palacci, S. Sacanna, A. Vatchinsky, P. M. Chaikin and D. J. Pine, *J. Am. Chem. Soc.*, 2013, **135**, 15978-15981.

25. S. Balasubramanian, D. Kagan, K. M. Manesh, P. Calvo-Marzal, G.-U. Flechsig and J. Wang, *Small*, 2009, **5**, 1569-1574.

26. Z. Wu, X. Lin, Y. Wu, T. Si, J. Sun and Q. He, *ACS Nano*, 2014, **8**, 6097-6105.

27. Z. Liu, J. Li, J. Wang, G. Huang, R. Liu and Y. Mei, *Nanoscale*, 2013, **5**, 1345-1352.

28. S. Sanchez, A. N. Ananth, V. M. Fomin, M. Viehrig and O. G. Schmidt, *J. Am. Chem. Soc.*, 2011, **133**, 14860-14863.

29. T. L. Xu, F. Soto, W. Gao, V. Garcia-Gradilla, J. X. Li, X. J. Zhang and J. Wang, *J. Am. Chem. Soc.*, 2014, **136**, 8552-8555.

30. F. Mou, C. Chen, H. Ma, Y. Yin, Q. Wu and J. Guan, *Angew. Chem. Int. Ed.*, 2013, **52**, 7208-7212.

31. F. Mou, C. Chen, Q. Zhong, Y. Yin, H. Ma and J. Guan, *ACS Appl. Mater. Interfaces*, 2014, **6**, 9897-9903.

32. W. Gao, A. Pei and J. Wang, *ACS Nano*, 2012, **6**, 8432-8438.

33. J. Li, V. V. Singh, S. Sattayasamitsathit, J. Orozco, K. Kaufmann, R. Dong, W. Gao, B. Jurado-Sanchez, Y. Fedorak and J. Wang, *ACS Nano*, 2014, **8**, 11118-11125.

34. A. A. Solovev, S. Sanchez and O. G. Schmidt, *Nanoscale*, 2013, **5**, 1284-1293.

35. T. Xu, F. Soto, W. Gao, R. Dong, V. Garcia-Gradilla, E. Magaña, X. Zhang and J. Wang, *J. Am. Chem. Soc.*, 2015, **137**, 2163-2166.

36. W. Gao, A. Pei, X. Feng, C. Hennessy and J. Wang, *J. Am. Chem. Soc.*, 2013, **135**, 998-1001.

37. X. Chen and S. S. Mao, *Chem. Rev.*, 2007, **107**, 2891-2959.

38. F. Mou, C. Chen, J. Guan, D.-R. Chen and H. Jing, *Nanoscale*, 2013, **5**, 2055-2064.

39. L. Li, L. Xu, W. Shi and J. Guan, *Int. J. Hydrogen. Energ.*, 2013, **38**, 816-822.

40. S. Eiden-Assmann, J. Widoniak and G. Maret, *Chem. Mater.*, 2004, **16**, 6-11.

41. K. He, G. Zhao and G. Han, *CrystEngComm*, 2014, **16**, 7881-7884.

42. M. Dahl, Y. Liu and Y. Yin, *Chem. Rev.*, 2014, **114**, 9853-9889.

43. Y. Ma, X. Wang, Y. Jia, X. Chen, H. Han and C. Li, *Chem. Rev.*, 2014, **114**, 9987-10043.

44. W. F. Paxton, A. Sen and T. E. Mallouk, *Chem. Eur. J.*, 2005, **11**, 6462-6470.

45. A. Yamakata, T.-a. Ishibashi and H. Onishi, *J. Phys. Chem. B*, 2001, **105**, 7258-7262.

46. J. L. Anderson, *Annu. Rev. Fluid. Mech.*, 1989, **21**, 61-99.

47. S. Shen, X. Wang, T. Chen, Z. Feng and C. Li, *J. Phys. Chem. C*, 2014, **118**, 12661-12668.

48. H.-R. Jiang, N. Yoshinaga and M. Sano, *Phys. Rev. Lett.*, 2010, **105**, 268302.

49. D. Yamamoto, A. Mukai, N. Okita, K. Yoshikawa and A. Shioi, *J. Chem. Phys.*, 2013, **139**, 034705.

Nanoscale Accepted Manuscript